A modeling assessment of the origin of Beryllium-7 and Ozone in the Canadian Rocky Mountains

R. D'Amours,[1,2] R. Mintz,[3] C. Mooney,[3] and B. J. Wiens[3]

Received 23 August 2012; revised 12 August 2013; accepted 13 August 2013; published 13 September 2013.

[1] This paper seeks to investigate the extent to which stratosphere-to-troposphere transport (STT) impacts the Canadian Rocky Mountain foothills. Beryllium-7 (^{7}Be) was monitored weekly at Harlech, Alberta, from July 2003 to June 2004, and daily during the spring of 2004. These data, together with hourly ozone (O_3) and relative humidity (RH) measurements, are presented and analyzed, with a focus on the spring of 2004. A Lagrangian dispersion model was used to help determine the origin of air parcels arriving at Harlech in order to assess if these periods were related to well-defined stratospheric intrusions. The modeling results show that events consisting of above average surface observations of ^{7}Be and O_3, and below average surface observations of RH, are the result of the arrival of air originating from the middle and upper troposphere. During the spring of 2004, no direct STTs were observed; all identified events were determined to be indirect STTs or middle to upper troposphere transport that occurred several days prior to being detected at Harlech. The most significant event occurred between 2 and 11 April, which had the longest period of elevated ^{7}Be and O_3 observations and the lowest RH measured during the spring of 2004, and where the modeling showed a strong stratospheric input. This input can be connected with two well-defined stratospheric intrusions occurring over the northern Pacific Ocean, more than 5 days before the associated surface observations. Furthermore, the modeling shows that periods of below average ^{7}Be and O_3 occurred when the station was mainly influenced by air masses circulating in the boundary layer.

Citation: D'Amours, R., R. Mintz, C. Mooney, and B. J. Wiens (2013), A modeling assessment of the origin of Beryllium-7 and ozone in the Canadian rocky mountains, *J. Geophys. Res. Atmos.*, *118*, 10,125–10,138, doi:10.1002/jgrd.50761.

1. Introduction

[2] There is general agreement that higher terrain, especially mountainous summits, are more frequently influenced by stratospheric intrusions. This is mainly due to elevation, but also in part to lee cyclogenesis generated by large mountain ranges [*Stohl et al.*, 2000; *Buzzi et al.*, 1984]. However, stratosphere-to-troposphere transport (STT) can also happen far upstream from a site [*Stohl et al.*, 2003], with its effects measured at the surface many hours or sometimes days after the occurrence of the STT. These events can be referred to as "indirect STTs" because they enrich the upper troposphere with stratospheric constituents, but other processes, such as a subsident flow over the lee side of mountain ranges, are required to transport these constituents to the surface. Again, high elevation sites are more likely to measure the impact of indirect STTs simply because they are closer to the middle or upper troposphere. Due to the province of Alberta's geographical location in the lee of the Canadian Rocky Mountains, there has been ongoing controversy in the Alberta air quality community regarding how much STT influences the province's surface ozone concentrations. In the absence of STT monitoring/modeling studies specific to Alberta, any conclusions drawn so far have been based on indirect inference from surface data [*Peake and Fong*, 1990]. This study was undertaken to help address this issue and to learn more about the nature of the STTs which affect Alberta.

[3] Many studies make use of beryllium-7 (^{7}Be) measurements to aid in identifying an STT signature. ^{7}Be is a radionuclide with a half-life of 53.3 days and is formed from spallation of nitrogen and oxygen nuclei by energetic particles associated with cosmic radiation entering the atmosphere [*Benioff*, 1956; *Lal et al.*, 1958; *Lal and Peters*, 1967; *Usoskin and Kovaltsov*, 2008]. The vertical concentration profile of ^{7}Be, which varies exponentially with altitude, depends mostly on its production rate which in turn depends on the depth of penetration of the cosmic particles having suitable energy. The largest ^{7}Be production rates and concentrations are typically found at altitudes above 20 km [*Lal and Peters*, 1967]. The availability of cosmic ray particles for ^{7}Be production also varies greatly with geomagnetic

[1]Department of Earth Sciences, University of Alberta, Edmonton, Alberta, Canada.
[2]Canadian Meteorological Centre, Edmonton, Québec, Canada.
[3]Meteorological Service of Canada, Environment Canada, Edmonton, Alberta, Canada.

Corresponding author: R. D'Amours, Department of Earth Sciences, University of Alberta, Edmonton, Alberta, Canada. (rdamours@ualberta.ca)

2169-897X/13/10.1002/jgrd.50761

latitude, with numbers increasing significantly toward the poles because of the redirection of initially isotropic incoming cosmic radiation by the Earth's magnetic field [*Brost et al.*, 1991; *Kritz et al.*, 1991]. Once formed, ^{7}Be atoms almost immediately attach to aerosol particles, and their fate becomes dependent on the future of these aerosols. In particular, ^{7}Be depletion in the troposphere is caused by processes such as precipitation washout and vertical and horizontal transport [*Feely et al.*, 1989]. The advantages and disadvantages of ^{7}Be as a stratospheric tracer are well documented [*Lal et al.*, 1958; *Lal and Peters*, 1967; *Feely et al.*, 1989; *Brost et al.*, 1991; *Kritz et al.*, 1991; *Jordan et al.*, 2003; *Zanis et al.*, 2003b]. The primary advantages are that a significant portion of ^{7}Be is produced in the stratosphere, and its relatively short half-life (53.3 days) restricts its formation and transport to synoptic and slightly longer timescales. Also, ^{7}Be is not created in significant amounts by processes other than spallation, which simplifies source attribution [*Usoskin et al.*, 2009]. An important restriction is that ^{7}Be production occurs in the upper troposphere as well as the stratosphere; nearly one third of the total production in the midlatitudes occurs below the tropopause [*Lal et al.*, 1958]. Another disadvantage is that ^{7}Be, because it is attached to aerosols, is subject to tropospheric removal processes, which complicates the assessment of surface concentrations. Many studies [e.g., *Dibb et al.*, 1994; *Jordan et al.*, 2003; *Zanis et al.*, 2003a] utilize the ratio ^{10}Be/^{7}Be to at least partially overcome this. Beryllium-10 (^{10}Be) is formed in the same manner as ^{7}Be, and in the same regions of the atmosphere, but has a very long half-life (1.5×10^{6} years) [*Zheng et al.*, 2011], and the ^{10}Be/^{7}Be ratio can be used as a stratospheric tracer not affected by tropospheric deposition processes [*Zheng et al.*, 2011]. Also, because of the different half-lives of the two components, their ratio can be used to roughly estimate the relative age of an air parcel, with air residing in the stratosphere for long periods having higher ratios [*Jordan et al*., 2003].

[4] The typical surface manifestations of a stratospheric intrusion event are well established: low relative humidity (RH), elevated O_3 concentrations, elevated ^{7}Be concentrations [*Elbern et al.*, 1997; *Stohl et al.*, 2000; *Cristofanelli et al.*, 2003], and high ratios of ^{10}Be/^{7}Be [*Dibb et al.*, 1994; *Jordan et al.*, 2003; *Zanis et al.*, 2003a]. Because of dilution and mixing with tropospheric air, STT events are not always associated with clearly elevated O_3 and low RH conditions [*Cristofanelli et al.*, 2003]. Pairing ^{7}Be and the ratio ^{10}Be/^{7}Be with O_3 and RH observations tends to give the best indication of potential stratospheric intrusion events. However, ^{10}Be data was not collected in this study, so similar to several other studies [e.g., *Stohl et al.*, 2000; *Cristofanelli et al.*, 2003], the combination of ^{7}Be with O_3 and RH was used to identify potential STT events.

[5] Modern long range transport models are also effective tools for the investigation of STT. Modeling approaches include the use of mean wind trajectories [*Bachmeier et al.*, 1994; *Stohl et al.*, 2000; *Colette et al.*, 2005], Lagrangian stochastic models [*Stohl et al.*, 2000; *Cristofanelli et al.*, 2003; *Cui et al.*, 2009], and Eulerian dispersion models [*Cristofanelli et al.*, 2003]. For example, Lagrangian models have been used to establish climatologies of STT events by initially distributing a large number of particles throughout the lower stratosphere and then running the model forward in time for long periods in order to describe STT temporally and spatially [*James et al.*, 2003; *Stohl et al.*, 2003]. Atmospheric transport models can also be executed in inverse mode (i.e., initialized at receptors) to not only determine probabilistically the source region of a tracer later observed at a receptor location but also to make estimates of the tracer source strength [*Flesch et al.*, 1995; *Pudykiewicz*, 1998; *Seibert and Frank*, 2004].

[6] This study investigates the extent to which STT impacts the foothills of the Canadian Rocky Mountains. During the spring of 2004, the monitoring of ^{7}Be was increased from weekly to daily at Harlech in the Alberta foothills. These data, together with hourly ozone (O_3) and RH measurements, are presented and analyzed. A Lagrangian particle dispersion model is used to investigate the origin of the observed ^{7}Be. The modeling study identifies potential source regions by using a metric, the layer residence time fraction, which is based on the time an air parcel spends above certain predefined vertical atmospheric levels, including the tropopause. Model results are compared to the surface-based observations to evaluate if STT can be associated with periods of elevated ^{7}Be and O_3 surface concentrations and of depressed RH.

2. Monitoring Site and Methodology

[7] The Harlech monitoring site is located at 52.569°N, 116.003°W, near the edge of the foothills region east of the Rocky Mountain range, at an elevation near 1600 m (Figure 1). The vegetation in the area is largely coniferous forest. Harlech is located near the hamlet of Nordegg (population $\sim$ 200), approximately 80 km west of Rocky Mountain House (population 6,874, Statistics Canada, 2007), and several hundred kilometers away from Alberta's major cities. There is a major highway (the David Thompson Highway) located 8 km south of Harlech. The elevations of the mountain peaks in the vicinity are slightly over 2000 m but can reach over 3000 m in the nearby Rocky Mountains. The area is used predominantly for camping, hiking, and outdoor recreation.

[8] Harlech ^{7}Be observations were taken from July 2003 to June 2004. Due to practical constraints, daily samples (24 h average) were only taken from March to June 2004; all other samples were weekly averages. Based on conclusions drawn by *Gerasopoulos et al.* [2001] and *Cristofanelli et al.* [2006], the March to June period was chosen for daily sampling, on the assumption that chances of detecting STT-related events were good. Despite the fact that the ratio ^{10}Be/^{7}Be is considered a more effective stratospheric tracer than ^{7}Be alone [*Zanis et al.*, 2003a; *Zheng et al.*, 2011], it was not possible to make measurements of ^{10}Be, again for practical reasons.

[9] Particulate matter was sampled with a high volume sampler using 3M F605 HEPA (high-efficiency particulate air)-rated (0.3 μm) filters. The sample filters were sent for analysis to SRC (Saskatchewan Research Council) Analytical Lab in Saskatoon, Saskatchewan, Canada. Gamma spectroscopy was used to analyze the collected aerosol on the filters for ^{7}Be, corrected for decay to the midpoint of the sample collection period. Since the daily ^{7} Be measurement start and end times were based on local time and varied slightly from day to day, a simple weighted average

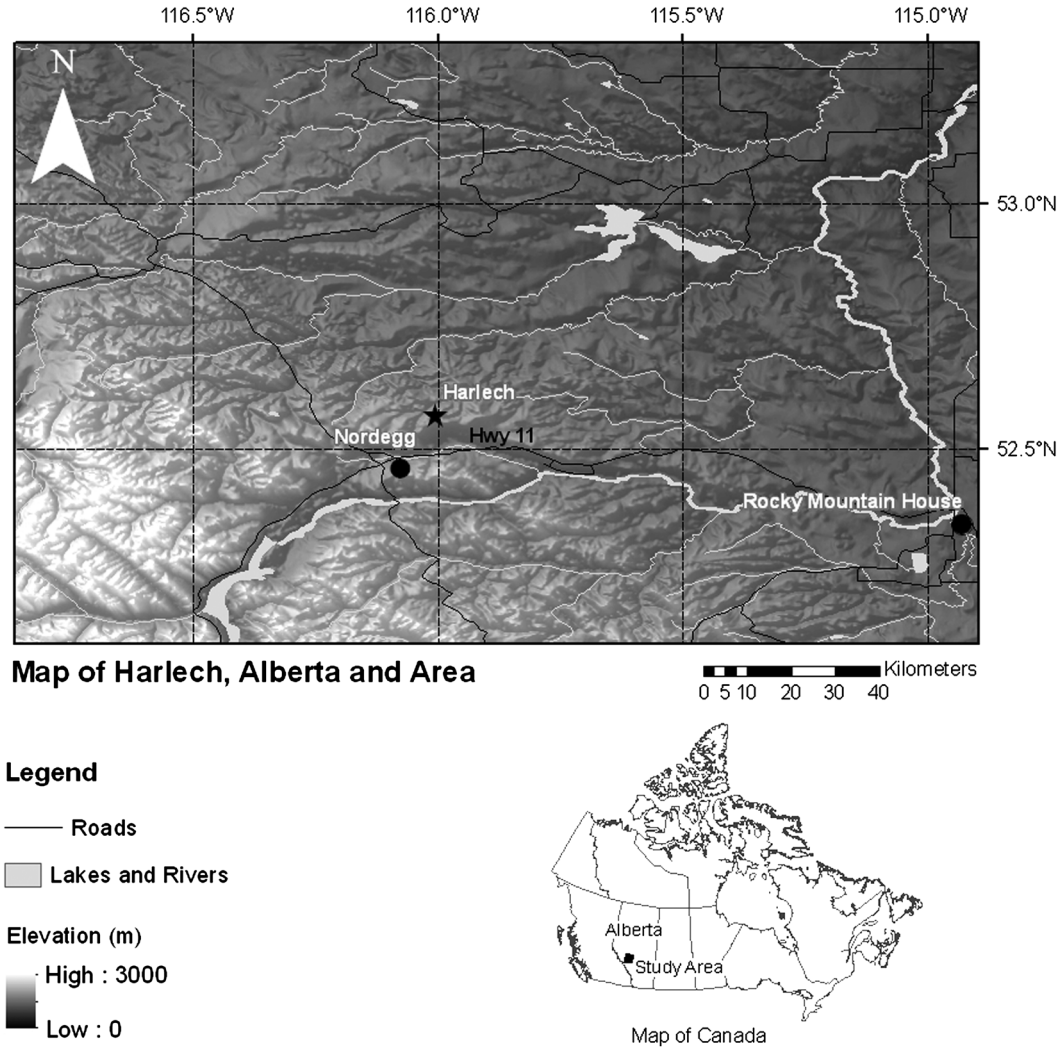

Figure 1. Map of the study area and location of the Harlech monitoring station.

was applied to derive a ^{7}Be time series where each data point represented a 24 h average starting and ending at 00:00 UTC.

[10] Ozone was sampled continuously at 5 min intervals throughout the entire period July 2003 to June 2004. Continuous O_3 measurements were made with a UV-absorption analyzer (TECO 49C). The O_3 analyzer was calibrated monthly, and span and zeros conducted daily. Data presented in the sections below has been transformed into hourly and daily averages from the 5 min data. RH observations along with other routine meteorological data were acquired on an hourly basis during the sampling period. RH was monitored because it is the variable of choice to represent atmospheric moisture content in STT studies, rather than specific humidity [*Stohl et al.*, 2000; *Cristofanelli et al.*, 2003]. This is primarily due to significantly higher variability of specific humidity compared to RH in the troposphere, with lower values in winter and in the upper atmosphere and higher values close to the surface and in warmer months [*Stohl et al.*, 2000]. The meteorological station equipment was colocated with the O_3 and ^{7}Be instruments and was calibrated monthly.

3. Overview of ^{7}Be and O_3 Data

[11] Monthly average ^{7}Be and O_3 concentrations measured at Harlech are shown in Figure 2. The highest ^{7}Be average is found in September (4.59 mBq m^{-3}); however, 75% of the data was missing for this month. Of the 32 weeks of weekly ^{7}Be monitoring (July 2003 to March 2004), a total of 8 weeks were missing from the months of August, September, October, and November 2003. The daily ^{7}Be data (March to June 2004) was 93% complete. Despite the fact that only 1 year of data is available, the annual cycle described by *Gerasopoulos et al.* [2001] and *Cristofanelli et al.* [2006] appears to be present and is seen in Figure 2, which shows a ^{7}Be maximum in late-summer.

[12] A statistical summary of O_3 and ^{7}Be concentrations measured at Harlech is presented in Table 1. Although ozone climatology varies from one alpine region to another, and distinct differences can be observed at sites separated by relatively short distances [*Stohl et al.*, 2000], studies conducted in the province of Alberta and in the Canadian Rocky Mountains by *Angle and Sandhu* [1986] and *Peake and Fong* [1990] can be compared to the Harlech data. The average

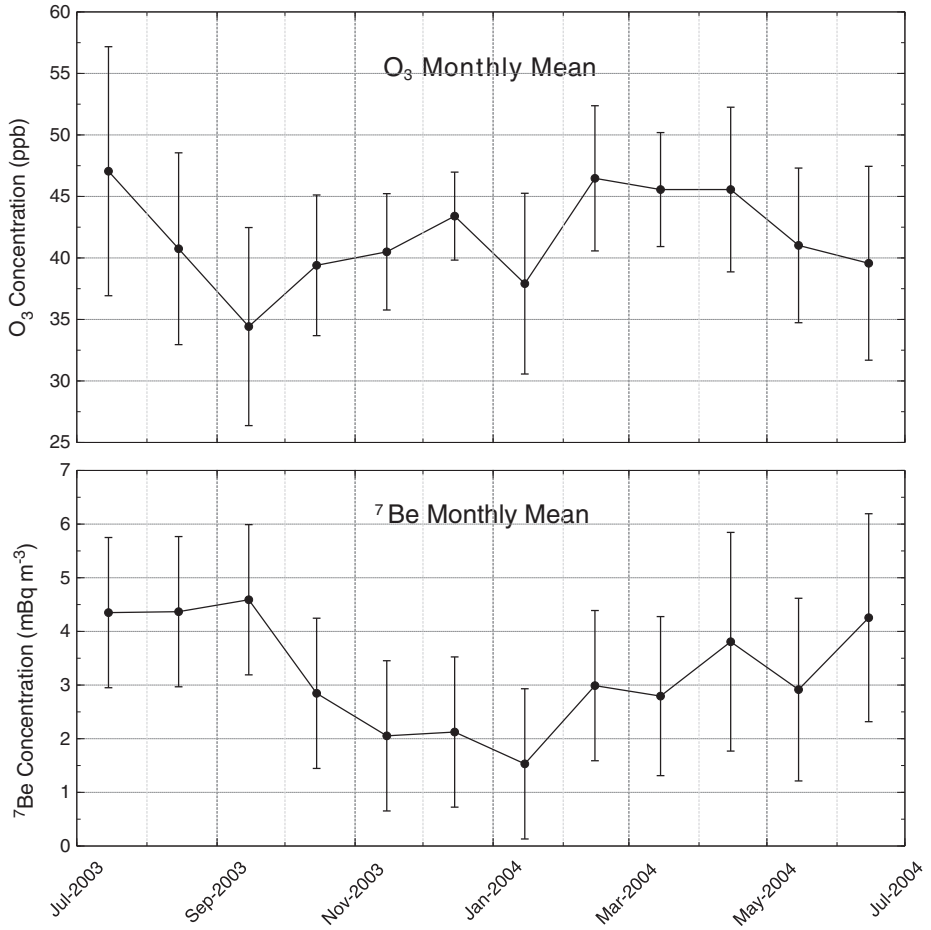

Figure 2. Monthly averages of ^{7}Be and O_3 concentrations measured at Harlech for July 2003 to June 2004. The O_3 error bars show the standard deviation of the daily means for each month. The ^{7}Be error bars use the standard deviation of all the weekly averages (1.39 mBq m^{-3}) from June 2003 to February 2004, and the standard deviation of the daily means of each month for March, April, May, and June 2004.

O_3 of 41 ppb and the median of 42 ppb in Harlech are close to the 43 ppb average and 41 ppb median of the nearly normally distributed data measured at the remote mountain site reported by *Peake and Fong* [1990]. The monthly averages in Harlech (Figure 2) show O_3 to have a late winter–early spring maximum (February–April) and a secondary summer maximum (July–August), but overall a relatively flat annual profile. This monthly profile is somewhat different from central European mountain sites which typically have a late spring maximum and winter minimum [*Logan*, 1985], but it does resemble the Alberta mountain site investigated by *Angle and Sandhu* [1986]. The highest monthly O_3 average at Harlech is found in February with an average of 46.5 ppb. The diurnal variation of hourly O_3 concentrations at Harlech over the July 2003 to June 2004 period is shown in Figure 3. The diurnal trend resembles the Alberta remote sites studied by *Angle and Sandhu* [1986] and *Peake and Fong* [1990], in which the trend is relatively flat. *Peake and Fong* [1990] compared the remote Canadian Rocky Mountain site at Fortress Mountain to two sites affected by a major urban center in the province of Alberta. The Fortress Mountain site had a small diurnal range (2.9 ppb), whereas the other two urban-affected sites had larger diurnal ranges of 11.6 and 16.5 ppb, which suggests that these sites were impacted by local photochemical production of O_3 and the associated diurnal NOx titration cycle. The ~5 ppb diurnal

Table 1. Statistical Summary of Hourly Average O_3 Concentrations for July 2003 to June 2004, Weekly ^{7}Be Concentrations, July 2003 to March 2004, and Daily ^{7}Be Concentrations, March to June 2004

	Hourly O_3 (ppb)	^{7}Be Weekly (mBq m^{-3})	^{7}Be Daily (mBq m^{-3})
Number of samples	7630	32	104
Average	41	2.76	3.39
Median	42	2.37	3.04
Range	80	4.54	7.23
Standard deviation	9	1.39	1.93
Maximum	88	5.46	7.61

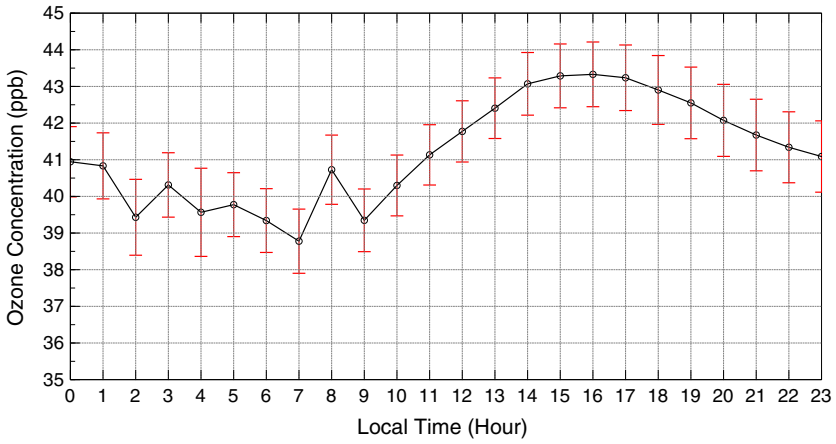

Figure 3. Mean diurnal variation of O_3 concentrations measured at Harlech for July 2003 to June 2004. The error bars represent the 95% confidence interval for each hourly mean.

range measured at Harlech is closer to the value determined for the remote mountain site investigated by *Peake and Fong* [1990], and thus is consistent with the assertion that Harlech is a relatively remote, pristine site, with no major anthropogenic sources that would lead to significant ozone production in the region.

[13] It is interesting to note that studies of the seasonality of STTs in the midlatitudes have shown discrepancies. Some studies have found spring and summer to have the highest likelihood of STTs [*Jordan et al.*, 2003; *Lefohn et al.*, 2011], while others have discussed sites where STTs were at a minimum in the summer [*Stohl et al.*, 2000]. Based on the monthly average plots shown in Figure 2 for ^{7}Be and O_3 measured at Harlech, it is reasonable to investigate the spring for STTs.

[14] Figure 4 shows time series of the daily average of ^{7}Be and O_3 concentrations and of RH, for the time period between March and June 2004. The correlations between the

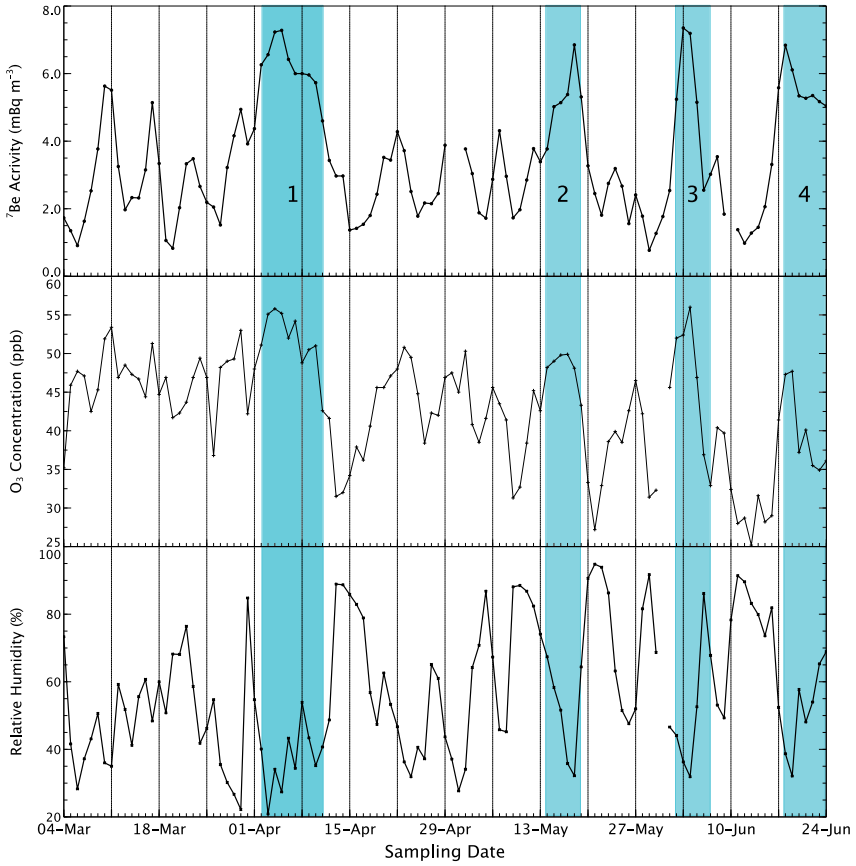

Figure 4. Daily averages of ^{7}Be, O_3, and RH at Harlech. The cyan colored areas, numbered 1 to 4, correspond to investigated events.

Table 2. Pearson Linear Correlation Coefficient ρ_P for Daily Mean ^{7}Be and O_3 Concentrations, Daily Mean RH

Observation Pair	ρ_P
^{7}Be–O_3	0.59
^{7}Be–RH	–0.51
O_3–RH	–0.80

three time series are shown in Table 2. In Figure 4, the larger peaks in ^{7}Be and O_3 are associated with localized minimums in RH, suggesting that those events are linked to subsiding (i.e., drying) air masses. This hypothesis is supported by the negative correlation of ^{7}Be and O_3 with RH (see Table 2).

[15] The autocorrelation within the ^{7}Be time series was assessed by correlating it to a lagged version of itself. With a 1 day lag, the correlation was greater than 0.8, while a 2 day lag resulted in a correlation below 0.5. A possible explanation for this phenomenon is that the effects of stratospheric intrusions often persist over several days, so that the autocorrelation over 1 or 2 day lag can be relatively strong.

[16] In addition, singular spectrum analysis (SSA), which is a tool used to identify quasiperiodic features in noisy time series [*Vautard and Ghil*, 1989; *Ghil et al.*, 2002], was applied to the detrended and normalized time series (using Analyseries, a time series analysis tool) [*Paillard et al.*, 1996]. Figure 5 shows the ^{7}Be and O_3 filtered time series. The correspondence between the two time series is very apparent and does support the idea that the same dynamic features contribute to increases in both ^{7}Be and O_3 concentrations in Harlech.

[17] Four events stand out in Figures 4 and 5, and are numbered 1 to 4 in Figure 4. These events, discussed in some detail in section 5.2, are characterized by the occurrence of one ^{7}Be daily observation greater than the 90th percentile. For all these events, O_3 is greater than 43 ppb (the O_3 average in spring 2004), and RH is less than 40% (the 20th percentile for RH in spring 2004). These values are similar to the subjective criteria for identifying STT events found in the literature [*Stohl et al.*, 2000; *Cristofanelli et al.*, 2003], which are based on elevated ^{7}Be and O_3, and depressed RH in relation to the region's seasonal averages/maximums.

4. Dispersion Modeling

4.1. Application of the Canadian Meteorological Centre Lagrangian Dispersion Model

[18] Lagrangian stochastic particle dispersion models simulate atmospheric dispersion by calculating the trajectories of a very large number of particles representing fluid elements. The effects of unresolved turbulent wind components are modeled through a stochastic Langevin equation (for velocity increments) or a random displacement equation (for displacement increments). For this study, the Canadian Meteorological Centre (CMC) Lagrangian particle dispersion model, MLDP0 (modèle Lagrangien de dispersion de particules d'ordre zéro), was executed in inverse mode. MLDP0 uses the random displacement equation (RDE) to model turbulent mixing. Models using the RDE are often referred to as "zeroth" -order models. A discussion of the RDE can be found, for example, in *van Dop et al.* [1985], *Boughton et al.* [1987], or *Wilson and Sawford* [1996]. Tracer depletion due to radioactive decay is modeled according to the usual exponential decay. Wet scavenging is modeled by utilizing a wet scavenging coefficient which is dependent on the cloud fraction at the location of the fluid particles; the wet scavenging rate is proportional to the tracer concentration, which leads to an exponential decay [*Pudykiewicz*, 1989]. Dry deposition occurs when a fluid element reaches the ground and is modeled in terms of a reflection probability as in *Wilson et al.* [1989]. This is to account for the fact that while fluid elements are reflected upward after reaching the ground, only a fraction of the associated beryllium aerosols is reflected back with the fluid elements, depending on the absorption characteristics of the surface. The reflection probability is a function of the deposition velocity normally used to characterize the flux of airborne substances from the atmosphere to the surface. Gravitational settling is modeled in terms of a terminal velocity for the particulates [*Sparks et al.*, 1997; *Durant and Rose*, 2009]. For ^{7}Be aerosols, however, it was considered negligible. More details as well as validation studies on MLDP0 can be found in R. D'Amours and A. Malo (A Zeroth Order Lagrangian Dispersion Model MLDP0, Internal Report, Canadian Meteorological Centre, 2004) and in *D'Amours et al.* [2010]. Simulations were done for each 24 h sample between 2 March and

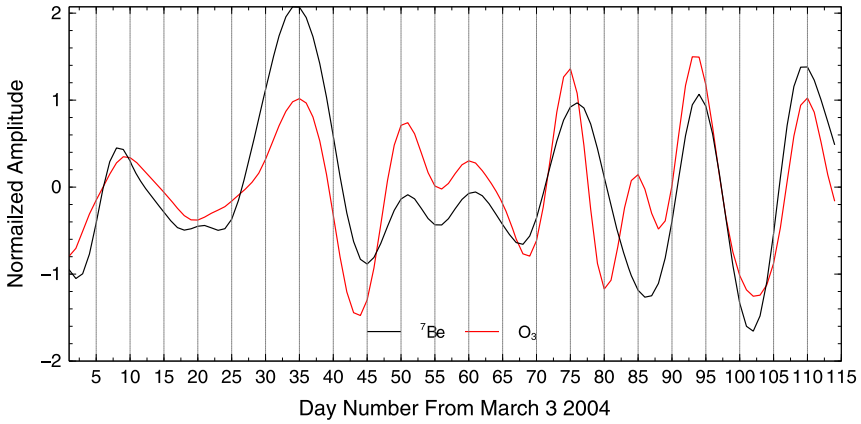

Figure 5. SSA filtered daily averages of ^{7}Be and O_3 at Harlech.

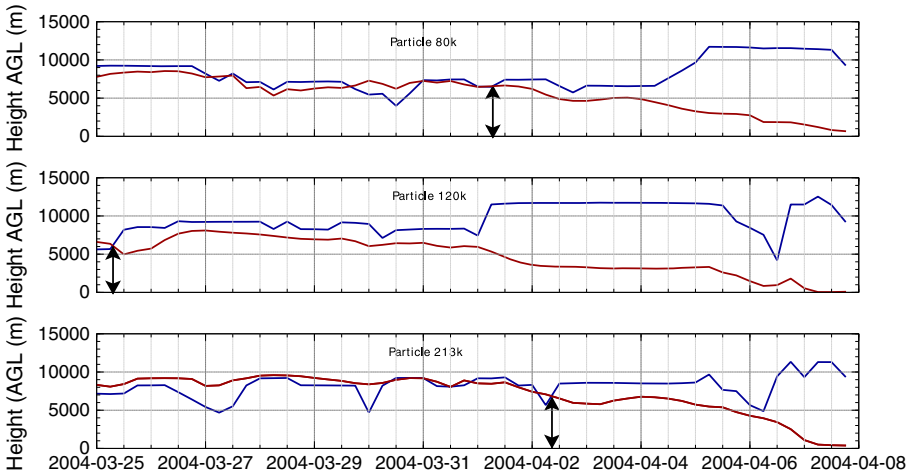

Figure 6. Vertical trajectories of selected particles, as a function of time, as they move toward the Harlech sampler. Sampling ends at 8 April 00 UTC. The dark red line represents the particle position, and the dark blue line represents the tropopause height (2 PVU level) at the particle position. The vertical arrows indicate the time when the particle exits the stratosphere for the last time. This defines the "exit time" used in the study.

26 June 2004. In each simulation, 864,000 particles were released continuously during the sampling period (24 h) from the observation site and tracked 14 days backward in time.

[19] The driving meteorological fields were provided by the CMC Global Environmental Multiscale (GEM) numerical weather prediction system [*Côté et al.*, 1998a, 1998b]. The horizontal resolution of the meteorological fields was approximately 100 km, with 58 η-levels in the vertical. MLDP0 was run with a global configuration, using a representative selection of 25 of these vertical η-levels, from $\eta = 1$ to $\eta = 0.027$ (i.e., surface to ~22 km above sea level).

4.2. Potential Source Layers for ^{7}Be

[20] Several potential ^{7}Be source layers were considered in this study. A stratospheric layer was delineated by diagnosing the tropopause height using the isentropic coordinate form of Ertel's potential vorticity [*Holton*, 1992]. In the literature, potential vorticity thresholds used to estimate tropopause height range between 1 and 3.5 potential vorticity units (PVU, 1 PVU = 1×10^{-6} m^2 K kg^{-1} s^{-1}) [*Bachmeier et al.*, 1994; *Holton et al.*, 1995; *Stohl et al.*, 2000; *Colette et al.*, 2005]. This study uses 2 PVU as the threshold, because observations indicate this metric provides a good estimate of the tropopause height in the midlatitudes [*Holton et al.*, 1995]. Other layers were also considered: above 10 km (>10 km), above 8 km (> 8 km), above 4 km (> 4 km), above 2 km (> 2 km), and less than ($\leqslant$ 2) km. The layers are terrain following, all elevations above ground level, and are not mutually exclusive. While the > 2 km layer was selected to account for any transport from above the planetary boundary layer (PBL), the > 4 km layer was chosen to investigate transport from the middle troposphere. The $\leqslant$ 2 km layer was considered to evaluate the effects of air masses circulating mainly in the PBL.

4.3. The Layer Residence Time Fraction

4.3.1. The Layer Residence Time

[21] The influence of the different layers on the samples taken at Harlech was estimated by means of a layer residence time fraction, $\overline{F_t^l}$. The $\overline{F_t^l}$ was determined by calculating the ratio of the total time particles spent in the layer of interest to the total duration of the particle trajectories over the course of the 14 day inverse simulation.

[22] The residence time, τ_p, for particle p above a certain vertical level z_l is defined as follows:

$$\tau_p(> z_l) = \int_{t_s}^{t_s - T_p} f(z_p, t)\mathrm{d}t, \tag{1}$$

where T_p is the particle's trajectory duration, t_s is the sampling time, and

$$f(z,t) = \begin{cases} 1 & z(t) \geq z_l \\ 0 & z(t) < z_l \end{cases}. \tag{2}$$

Finally, an average ratio for the total number, N, of particles used in the simulation is calculated as follows:

$$\overline{F_t^l} = \frac{1}{N}\sum_{p=1}^{N} \frac{\tau_p(> z_l)}{T_p}. \tag{3}$$

[23] The concept of residence time is illustrated in Figure 6, which shows the vertical position of three particles as a function of time along their 14 day trajectory. These particles were chosen because they follow fairly different vertical trajectories and illustrate that particles can move in and out of the stratosphere several times during 14 days in different ways. Particle 80k moves in and out of the stratosphere during the early part of its trajectory then permanently moves below the tropopause after 1 April, on its descent toward Harlech. Particle 120k starts above the tropopause on the first day of its 14 day trajectory then quickly crosses into in the upper troposphere (above 5 km)

where it remains for nearly a week. On the other hand, particle 213k travels in the lower part of the stratosphere for more than 5 days, then moves very near the tropopause level for about 3 days, finally descending into the troposphere on 2 April. The $\tau_p(z_l > 2$ PVU) value for particle 120k would be less than 1 day, while it would be nearly 6 days for particle 213k.

[24] It is easily seen from Figure 6 how an estimation of the time at which particles exit a layer of interest can be obtained. The "exit time" for a particle is defined as the time at which the particle crosses a layer boundary for the last time before traveling to the Harlech sampler. The number of particles exiting a layer, using that definition, is calculated for each 6 h period of the inverse simulation. The layer exit rate is defined as the ratio of the number of particles exiting a layer to the total number of particles used in the simulation.

4.3.2. Weighted Residence Time

[25] The particles are emitted from the receptor at sample time t_s with an initial weight $m_p(t_s)$ which represents the relative importance of the particle in the sample. For example, if the sample is represented by N particles of equal weight, $m_p(t_s)$ could be chosen as $1/N$. This weight is reduced as a particle moves backward (from t_s) on its trajectory because of radioactive decay, wet scavenging, and dry deposition. Hence, at a time $t < t_s$, a particle's weight $m_p(t)$ is lower than it was at t_s. Since individual trajectories may differ significantly, the effect of the last two processes will also differ for different trajectories, ultimately resulting in a change in the relative contribution of each particle to the sample. A mass weighted residence time is calculated for each particle as follows:

$$\tau_p^w(> z_l) = \int_{t_s}^{t_s - T_p} \frac{m_p(t)}{m_p(t_s)} f(z,t)\mathrm{d}t\,. \tag{4}$$

A ratio of the individual particle's mass weighted residence time to the total trajectory duration is then obtained with:

$$W_p^l = \frac{\tau_p^w(> z_l)}{T_p}\,, \tag{5}$$

and an average ratio for the total number, N, of particles used in the simulation is calculated similarly to equation (3):

$$\overline{W_t^l} = \frac{1}{N}\sum_{p=1}^{N} W_p^l\,. \tag{6}$$

$\overline{W_t^l}$ defines the weighed layer residence time fraction.

[26] Assuming that all the ^{7}Be measured in the sample originated from the layer above z_l, the average weighted residence time given by equation (3) could be used to estimate the ^{7}Be concentration in that potential source layer. Inverse Lagrangian stochastic dispersion modeling is often used in a similar fashion to estimate the source characteristics of an atmospheric tracer observed at one or more receptor points [*Flesch et al.*, 1995; *Wotawa et al.*, 2003]. However, the main purpose for calculating $\overline{F_t^l}$ and $\overline{W_t^l}$ in this study is to assess the relative importance of the layers as potential sources for ^{7}Be measured at Harlech and to look for connections between surface observations at Harlech and potential stratospheric/upper tropospheric input to those observations. The only hypothesis made is that the impact of the potential source layers on the nature of the air particles reaching the sampler can be related to the time spent in those layers.

5. Analysis of the Modeling Results

5.1. Comparison of ^{7}Be and O_3 Concentrations to the Layer Residence Time Fraction

[27] Figure 7 shows the time series of $\overline{W_t^l}$ derived from the MLDP0 results for various layers, with the corresponding observed ^{7}Be concentration time series. The $\overline{W_t^l}$ values for the > 10 km layer are relatively small during the study period, indicating that there was little air originating from the > 10 km layer (for any time during the 14 days prior to the observation) which was ultimately sampled at Harlech. On the other hand, the $\overline{W_t^l}$ values for the > 8 km layer and for the stratosphere as defined by the > 2 PVU level, although not very large, are often appreciable, especially in March and April, and correlate with episodes of elevated ^{7}Be concentrations. The greatest contribution from the > 8 km and > 2 PVU layers occurs for the 24 h sample ending 8 April 00 UTC, which had the second highest ^{7}Be concentrations measured during the study period. For the three other elevated ^{7}Be and O_3 events, the > 8 km and > 2 PVU layer $\overline{W_t^l}$ values show local maxima but to a lesser extent than those values determined for event 1 (2–11 April).

[28] Table 3 shows the Pearson linear correlation coefficient, ρ_P, between the $\overline{W_t^l}$ time series shown in Figure 7 and ^{7}Be and O_3 concentrations. Table 3 also shows ρ_P for the $\overline{F_t^l}$ time series (where depletion processes are not considered) and ^{7}Be and O_3 daily concentrations. There is little correlation between ^{7}Be concentrations and $\overline{W_t^l}$ for the layer below 2 km. In contrast, the correlation between ^{7}Be and $\overline{F_t^l}$ is strongly negative, meaning that when air, which has been traveling near the surface for a significant portion of the preceding 14 days, reaches the sampler, there is an important drop in the ^{7}Be concentrations. However, modeling removal mechanisms essentially decouples ^{7}Be concentrations from the $\leqslant$ 2 km layer. This is a good indication that the ^{7}Be content of that air is typically very low. In the bottom panel of Figure 7, the $\overline{W_t^l}$ values for the > 2 km and the > 4 km layers generally track the ^{7}Be observations quite well throughout the monitoring period and show the highest correlations, even when there does not seem to be much contribution from the upper layers associated with them. Table 3 also shows that ρ_P values are similar and fairly high for the $\overline{W_t^l}$ from the layers > 4 km and > 2 km; correlations for $\overline{F_t^l}$ are also significant but lower than those for $\overline{W_t^l}$, indicating that there is information gained by modeling the removal mechanisms. For the > 10 km, > 8 km, and > 2 PVU layers, the correlations between ^{7}Be and $\overline{W_t^l}$, and between ^{7}Be and $\overline{F_t^l}$ are still important, but relatively less so than for the lower layers. These smaller correlations indicate that, on average and over a 14 day period, input from the > 10 km, > 8 km, and > 2 PVU layers is not the most important contributor to ^{7}Be measured at Harlech, rather they suggest transport from within the middle troposphere has the most significant effect.

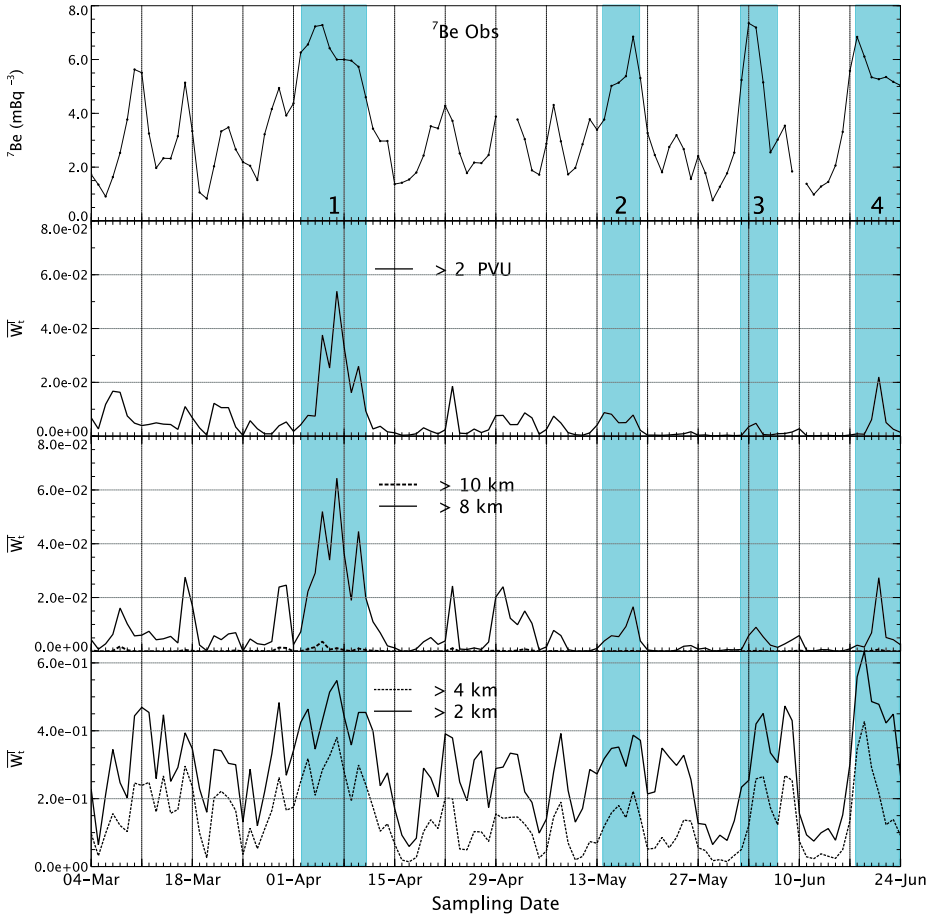

Figure 7. Observations of (top) ^{7}Be daily average concentrations compared to the weighted layer residence time fraction, $\overline{W_t^l}$, for various layers during the period March to June 2004. Note the scale differences in the $\overline{W_t^l}$ values on the different panels. The cyan colored areas, numbered 1 to 4, correspond to investigated events.

[29] Due to the complexity of O_3 chemistry, there was no attempt in this study to model O_3 production or removal processes which may have helped clarify the relative contribution from the different layers. Nevertheless, correlations were calculated between the $\overline{F_t^l}$ and O_3 concentrations and show a pattern similar to correlations between $\overline{F_t^l}$ and ^{7}Be: negative for the layer $\leqslant$ 2 km and positive for the layers above. It would appear that input from the middle to upper troposphere and lower stratosphere has a significant effect on surface O_3 concentrations. In addition, the correlations indicate that, at Harlech, when air from above 2 km (normally from above the boundary layer) is transported to the surface, ^{7}Be and O_3 concentrations generally increase, whether or not stratospheric influx is detectable in the previous 14 days. When air originates mostly from the boundary layer, concentrations decrease. These findings support the idea that O_3 observed in the Alberta foothills is often, if not mostly, the result of transport to the surface from above the boundary layer and that input from the stratosphere and upper and middle troposphere has significant impact.

Table 3. Pearson Linear Correlation Coefficient ρ_P Between the Weighted Layer Residence Time Fraction, $\overline{W_t^l}$ and Daily ^{7}Be, Unweighted Layer Residence Time Fraction $\overline{F_t^l}$ (Radioactive Decay and Other Removal Processes are not Considered), and Daily ^{7}Be and O_3 Concentrations, for March to June 2004

Layer	$\overline{W_t^l}$ ^{7}Be	$\overline{F_t^l}$ ^{7}Be	$\overline{F_t^l}$ O_3
$\leqslant$ 2 km	–0.15	–0.64	–0.52
> 2 km	0.72	0.64	0.53
> 4 km	0.71	0.63	0.60
> 8 km	0.56	0.53	0.47
> 10 km	0.36	0.34	0.32
> 2 PVU	0.42	0.38	0.42

5.2. A Closer Look at the Four Potential STT Events

[30] Figure 8 shows the exit rates from the > 2 PVU and > 8 km layers, for one specific sampling day for each of the four events identified in Figures 4 and 7. The time series go back 14 days, at 6 h intervals, for the 24 h sampling period ending at the date/time indicated on the label.

[31] Figure 4 shows a clear rise in ^{7}Be and O_3, and a significant drop in RH during the 2–11 April period (event 1). This period also corresponds to the largest $\overline{W_t^l}$ from the > 8 km and > 2 PVU layers (Figure 7). The top left panel of Figure 8 shows that the stratospheric air parcels

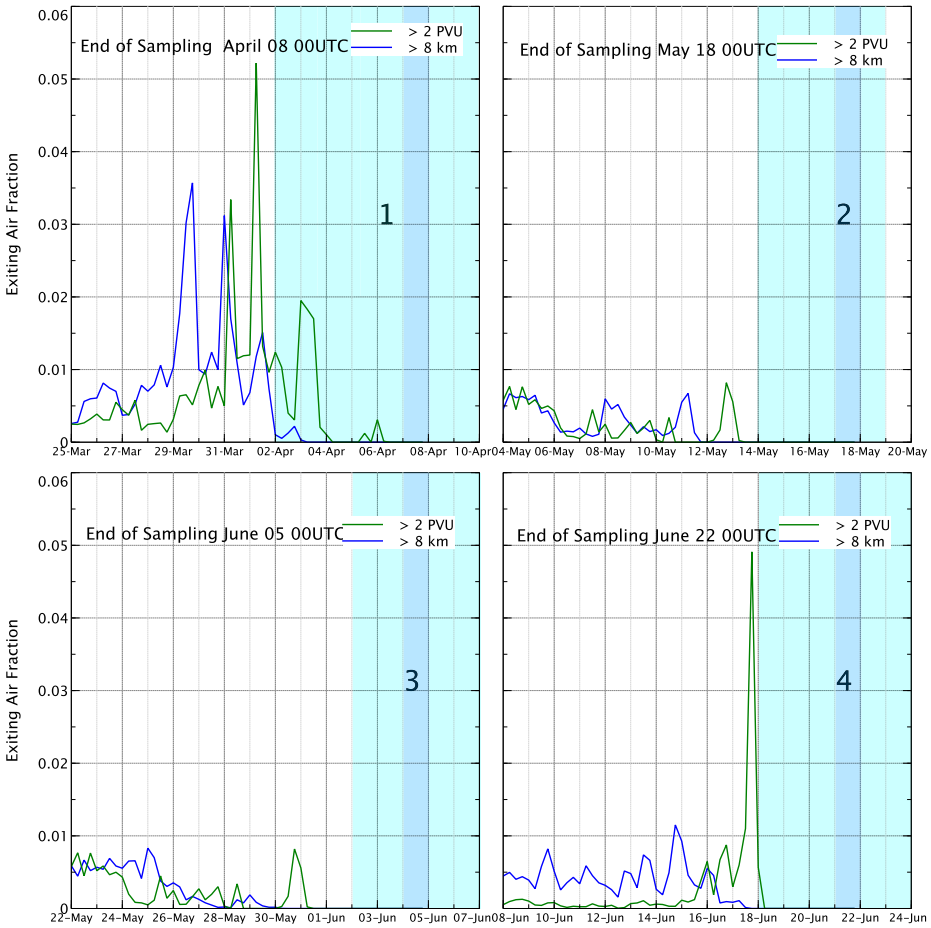

Figure 8. Layer exit rates for specific sampling days during the four investigated events. The layer exit rate is defined as the ratio of the number of particles exiting a layer for the last time, during a 6 h period, to the total number of particles used in the simulation (864,000). The areas colored in cyan indicate the total duration of the associated event (see Figure 7), while the blue colored areas show the duration of the sampling period for the specific day.

sampled during the 24 h period ending 8 April 00 UTC, actually exited the stratosphere (> 2 PVU layer) almost entirely between 29 March and 4 April. The strongest efflux occurred on 1 April. This indicates that a significant amount of time passed between the injection of stratospheric air in the troposphere and the time when elevated O_3 and ^{7}Be concentrations were measured at Harlech. It is also interesting to note that the peaks in the stratospheric exit rates are preceded

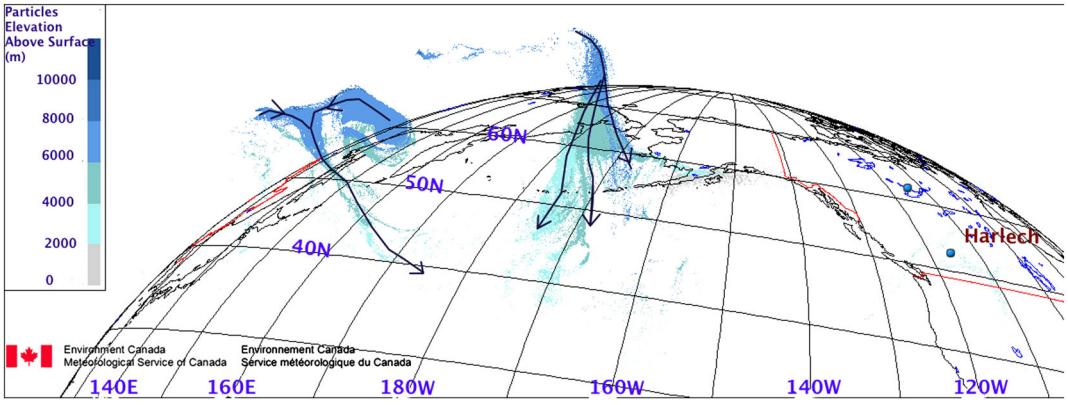

Figure 9. Position of the stratospheric particles (i.e., particles that have been above the 2 PVU level at least once), sampled at Harlech during a 24 h period ending 8 April 00 UTC. The arrows indicate the instantaneous motion and direction of the particles, 2 April 00 UTC, as they move toward Harlech.

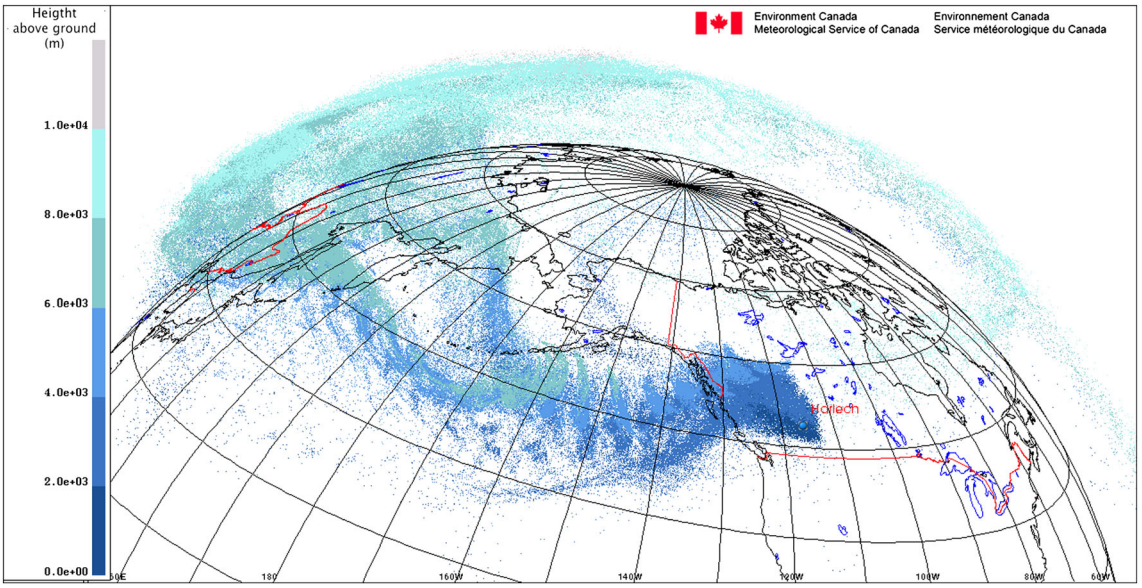

Figure 10. Time-integrated plume of the stratospheric particles (i.e., particles that have been above the 2 PVU level at least once), sampled at Harlech during the 24 h period ending 8 April 00 UTC. Particles were sampled from a reduced set of all the particles used in the simulation and are shown every 6 h during their 14 day trajectory toward Harlech.

by peaks nearly equally spaced in time in the > 8 km exit rates, indicating that air parcels were exiting the > 8 km layer many hours before crossing the tropopause. Therefore, it is likely that the tropopause was below 8 km (quite low) in the vicinity of the particle stratospheric exits, which is consistent with a deep upper trough, a common region for STT occurrences.

[32] Figure 9 depicts the particle positions at 2 April 00UTC, as they descend towards lower levels, en route to Harlech. This still image is associated with the simulation ending 8 April 00 UTC, and shows only the particles that were above the 2 PVU level at some time during the simulation, i.e., "stratospheric" particles. Figure 10 shows the time-integrated plume formed by those "stratospheric" particles as they move to the Harlech sampler. Clearly, the stratospheric efflux is related to two distinct and well separated events. The two largest peaks seen in the particle exit rates are produced by two descending streams which can be related to the two deep surface low pressure systems seen in Figure 11, also valid at 2 April 00 UTC. These two systems are associated with two well-developed cyclonic upper level systems marked by high values of potential vorticity at the 6000 m level shown on the same chart. Figure 12 shows a cross-section through the well-developed upper trough south of the Aleutians. There is a strong subsiding stream on the west side of the trough, with large downward vertical motions in what has all the appearances of a well-developed tropopause fold, where the 2 PVU surface

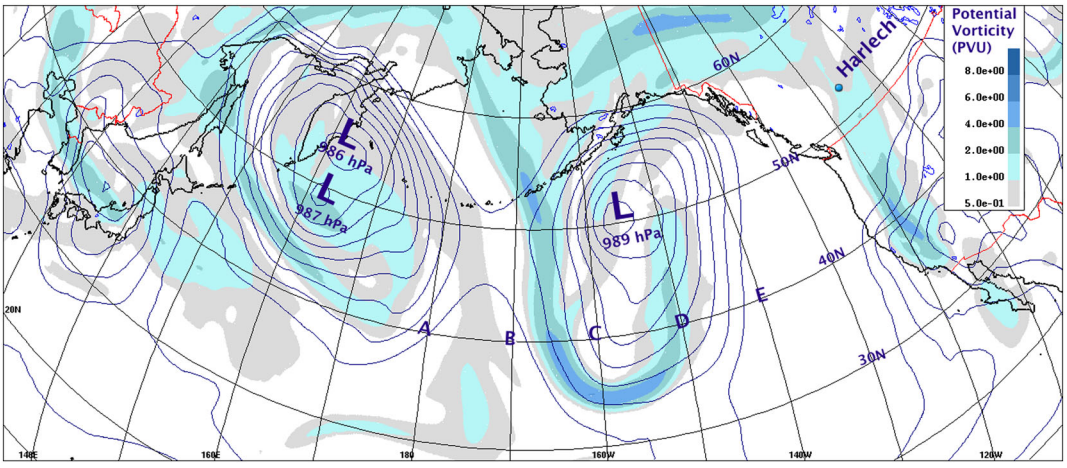

Figure 11. Potential vorticity (PV) 6000 m above the surface (color shading) and mean sea level pressure (continuous lines) valid 2 April 2004 00 UTC. The depth of the Pacific low pressure centers is shown in hPa, and the approximate position of the lowest pressure is indicated by a "L." A cross-section of the 3-D PV field along latitude 40°N, from points labeled A to E is shown in Figure 12.

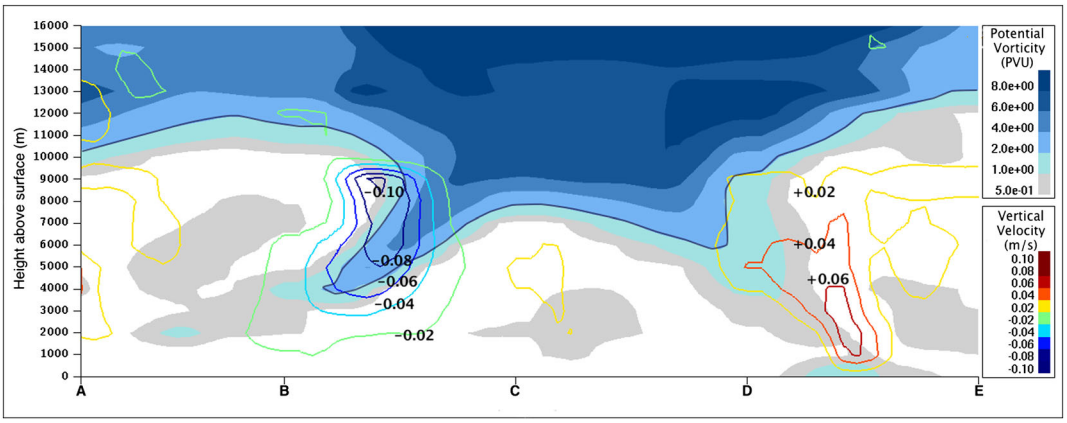

Figure 12. Cross section of the potential vorticity in PVU and of the vertical motion in m s^{-1}, shown by contour lines, along latitude 40°N valid 2 April 2004 00 UTC. The positions labeled A to E on the horizontal axis correspond to those in Figure 11. The continuous dark line delineates the tropopause according to the 2 PVU threshold.

lowers below 4000 m under a higher, second tropopause near 11000 m. This is where the model particles were descending, eventually making their way into the troposphere.

[33] The top right-hand and lower left-hand panels in Figure 8 show the fraction of exiting particles and their exit times for simulations associated with events 2 and 3. In these cases, the contribution from the > 8 km layer as well as that from the stratosphere (> 2 PVU), are much less than for event 1, but still clearly detected by the modeling. A possible explanation is that ^{7}Be concentrations in the source areas for these events are higher. Another possible explanation is that important STT events occurred before the 14 day backward trajectory period. However, a deeper investigation was beyond the scope of this study. In both cases, the transfers occurred over a fairly long period, more than a week, many days before sampling. The lower right-hand panel in Figure 8 (event 4) indicates a relatively important input from the > 8 km layer, which also occurred over several days, long before sampling but there is a sharp burst from the > 2 PVU layer on 17 June.

[34] The exit rate plots in Figure 8 highlight the need to distinguish between the actual stratospheric intrusion events which transport stratospheric particles into the troposphere and the observation of this stratospheric air at a surface site. In all cases of significantly elevated ^{7}Be in this study period, the STT events occurred several days before their impact was observed at the Harlech station. This finding is consistent with comments made by *Davies and Schuepbach* [1994] and *Stohl et al.* [2000] on indirect STT events which are only seen at the surface after the passage of several days. In addition, *Cui et al.* [2009] ran forward Lagrangian simulations for longer than 10 days and found a higher frequency of occurrence of STT events that took more than 4 days to reach the surface versus STT events that took less than 4 days to reach the surface. The MLDP0 simulations suggest that, for this data set, several STT events act to enrich the upper and middle troposphere with higher concentrations of ^{7}Be and O_3, and that it is this enriched air which is seen at the surface several days later and several thousand kilometers away from the original STT events. Direct stratospheric intrusion events (i.e., where a tropopause fold actually makes contact with the ground) occurring near a site and whose impact is seen immediately at the surface, are actually relatively rare [*Stohl et al.*, 2003]. None were observed near Harlech during the study period. The investigation of the individual events (results presented in Table 3 and discussed in section 5.1), provides significant evidence that long range transport from the middle and upper troposphere makes the greatest contribution to the elevated ^{7}Be and O_3 concentrations.

6. Summary and Conclusions

[35] ^{7}Be was monitored weekly at Harlech, Alberta, from July 2003 to June 2004, and daily during the spring of 2004. These data, together with hourly O_3 and RH measurements, were presented and analyzed, with a focus on the spring of 2004. The Lagrangian particle dispersion model MLDP0, run in inverse mode, was used to assess the influence of air parcels originating from different layers in the atmosphere on the concentrations observed during that period. The analysis was mainly done by evaluating the relative contribution of the different atmospheric layers, using a metric developed for this purpose, the layer residence time fraction $\overline{F_t^l}$ and the weighted layer residence time fraction $\overline{W_t^l}$. Other metrics used include the rate at which the parcels finally exit the layer before reaching the observation site (the exit rate) and the time when these occur, the exit time.

[36] MLDP0 model results show that at Harlech, above average observations of ^{7}Be and O_3, and below average observations of RH, are significantly correlated with the arrival at the surface of air originating from the middle and upper troposphere. Generally, there is a small contribution from particles originating from either the > 8 km or > 2 PVU layers, or both. The 2–11 April event, which had the longest period of elevated ^{7}Be and O_3 observations and the lowest RH recorded in the study, is the period where the model shows the strongest contribution from > 8 km and > 2 PVU layers. This can be related to two well-identified stratospheric intrusions occurring over the northern Pacific Ocean, more than 5 days before the associated observations. Three other events

were also identified. In these cases, the elevated ^{7}Be cannot be clearly attributed to STT occurring in the 14 day period prior to observations, but it can be attributed to the impact of middle tropospheric air subsiding into the site. The modeling also shows that periods of below average ^{7}Be and O_3 occurred when the station was mainly influenced by air masses circulating in the boundary layer. Correlations between $\overline{W_t^l}$, $\overline{F_t^l}$, and the ^{7}Be and O_3 concentrations support the view that episodes of elevated ^{7}Be and O_3, and depressed RH, observed in the Alberta foothills are typically the result of long range transport from the middle or upper troposphere, or from STTs, that have occurred several days and thousands of kilometers away from the observation site.

[37] In the future, a longer term field study which includes measurements of ^{10}Be as well as ^{7}Be at several sites would help clarify the nature and age of stratospheric and upper tropospheric input to the surface observations of O_3 in Alberta. Further modeling is needed to better understand the impact of trans-Pacific transport of anthropogenic O_3 on the Alberta O_3 budget.

[38] **Acknowledgments.** The authors would like to thank Dan McLennan for his help preparing Figure 1, and Laurie Bates-Frymel and Karen McDonald for their help with the initial project design. The authors appreciated the cooperation of Parkland Airshed Management Zone (PAMZ) on data collection at the Harlech site. Comments and suggestions from two anonymous reviewers improved the paper significantly.

References

Angle, R. P., and H. S. Sandhu (1986), Rural ozone concentrations in Alberta, Canada, *Atmos. Environ. (1967)*, *20*(6), 1221–1228, doi:10.1016/0004-6981(86)90157-5.

Bachmeier, A. S., M. C. Shipham, E. V. Browell, W. B. Grant, and J. M. Klassa (1994), Stratospheric/tropospheric exchange affecting the northern wetlands regions of Canada during summer 1990, *J. Geophys. Res.*, *99*(D1), 1793–1804, doi:10.1029/93JD02179.

Benioff, P. A. (1956), Cosmic-ray production rate and mean removal time of beryllium-7 from the atmosphere, *Phys. Rev.*, *104*(4), 1122–1130.

Boughton, B. A., J. M. Delaurentis, and W. E. Dunn (1987), A stochastic model of particle dispersion in the atmosphere, *Boundary Layer Meteorol.*, *40*(1), 147–163, doi:10.1007/BF00140073.

Brost, R. A., J. Feichter, and M. Heimann (1991), Three-dimensional simulation of ^{7}Be in a global climate model, *J. Geophys. Res.*, *96*(D12), 22,423–22,445, doi:10.1029/91JD02283.

Buzzi, A., G. Giovanelli, T. Nanni, and M. Tagliazucca (1984), Study of high ozone concentrations in the troposphere associated with lee cyclogenesis during ALPEX, *Beitr. Phys. Atmos.*, *57*, 380–392.

Colette, A., Gérard Ancellet, and F. Borchi (2005), Impact of vertical transport processes on the tropospheric ozone layering above Europe. Part I: Study of air mass origin using multivariate analysis, clustering and trajectories, *Atmos. Environ.*, *39*(29), 5409–5422, doi:10.1016/j.atmosenv.2005.06.014.

Côté, J., J.-G. Desmarais, S. Gravel, A. Méthot, A. Patoine, M. Roch, and A. Staniforth (1998a), The operational CMC–MRB global environmental multiscale (GEM) model. Part II: Results, *Mon. Weather Rev.*, *126*(6), 1397–1418, doi:10.1175/1520-0493(1998)126<1397:TOCMGE>2.0.CO;2.

Côté, J., S. Gravel, A. Méthot, A. Patoine, M. Roch, and A. Staniforth (1998b), The operational CMC–MRB global environmental multiscale (GEM) model. Part I: Design considerations and formulation, *Mon. Weather Rev.*, *126*(6), 1373–1395, doi:10.1175/1520-0493(1998)126<1373:TOCMGE>2.0.CO;2.

Cristofanelli, P., P. Bonasoni, L. Tositti, U. Bonafe, F. Calzolari, F. Evangelisti, S. Sandrini, and A. Stohl (2006), A 6-year analysis of stratospheric intrusions and their influence on ozone at Mt. Cimone (2165 m above sea level), *J. Geophys. Res.*, *111*, D03306, doi:10.1029/2005JD006553.

Cristofanelli, P., et al. (2003), Stratosphere-to-troposphere transport: A model and method evaluation, *J. Geophys. Res.*, *108*(D12), 8525, doi:10.1029/2002JD002600.

Cui, J., M. Sprenger, J. Staehelin, A. Siegrist, M. Kunz, S. Henne, and M. Steinbacher (2009), Impact of stratospheric intrusions and intercontinental transport on ozone at Jungfraujoch in 2005: Comparison and validation of two Lagrangian approaches, *Atmos. Chem. Phys.*, *9*(10), 3371–3383.

D'Amours, R., A. Malo, R. Servranckx, D. Bensimon, S. Trudel, and J.-P. Gauthier-Bilodeau (2010), Application of the atmospheric Lagrangian particle dispersion model MLDP0 to the 2008 eruptions of Okmok and Kasatochi volcanoes, *J. Geophys. Res.*, *115*, D00L11, doi:10.1029/2009JD013602.

Davies, T. D., and E. Schuepbach (1994), Episodes of high ozone concentrations at the Earth's surface resulting from transport down from the upper troposphere/lower stratosphere: A review and case studies, *Atmos. Environ.*, *28*(1), 53–68, doi:10.1016/1352-2310(94)90022-1.

Dibb, J. E., L. D. Meeker, R. C. Finkel, J. R. Southon, M. W. Caffee, and L. A. Barrie (1994), Estimation of stratospheric input to the Arctic troposphere: ^{7}Be and ^{10}Be in aerosols at Alert, Canada, *J. Geophys. Res.*, *99*(D6), 12,855–12,864, doi:10.1029/94JD00742.

Durant, A. J., and W. I. Rose (2009), Sedimentological constraints on hydrometeor-enhanced particle deposition: 1992 eruptions of Crater Peak, Alaska, *J. Volcanol. Geotherm. Res.*, *186*(1-2), 40–59, doi:10.1016/j.jvolgeores.2009.02.004.

Elbern, H., J. Kowol, R. Sladkovic, and A. Ebel (1997), Deep stratospheric intrusions: A statistical assessment with model guided analyses, *Atmos. Environ.*, *31*(19), 3207–3226.

Feely, H. W., R. J. Larsen, and C. G. Sanderson (1989), Factors that cause seasonal variations in beryllium-7 concentrations in surface air, *J. Environ. Radioact.*, *9*(3), 223–249.

Flesch, T. K., J. D. Wilson, and E. Yee (1995), Backward-time Lagrangian stochastic dispersion models and their application to estimate gaseous emissions, *J. Appl. Meteorol.*, *34*(6), 1320–1332, doi:10.1175/1520-0450(1995)034<1320:BTLSDM>2.0.CO;2.

Gerasopoulos, E., et al. (2001), A climatology of ^{7}Be at four high-altitude stations at the Alps and the Northern Apennines, *Atmos. Environ.*, *35*(36), 6347–6360, doi:10.1175/1520-0450(1995)034<1320:BTLSDM>2.0.CO;2.

Ghil, M., et al. (2002), Advanced spectral methods for climatic time series, *Rev. Geophys.*, *40*, 3-1–3-41.

Holton, J. R. (1992), *An Introduction to Dynamic Meteorology, International Geophysics Series* third ed., vol. 48, Academic Press, 1250 Sixth Avenue, San Diego, California.

Holton, J. R., P. H. Haynes, M. E. McIntyre, A. R. Douglass, R. B. Rood, and L. Pfister (1995), Stratosphere-troposphere exchange, *Rev. Geophys.*, *33*(4), 403–439, doi:10.1029/95RG02097.

James, P., A. Stohl, C. Forster, S. Eckhardt, P. Seibert, and A. Frank (2003), A 15-year climatology of stratosphere-troposphere exchange with a Lagrangian particle dispersion model 2. Mean climate and seasonal variability, *J. Geophys. Res.*, *108*(D12), 8522, doi:10.1029/2002JD002639.

Jordan, C. E., J. E. Dibb, and R. C. Finkel (2003), ^{10}Be/^{7}Be tracer of atmospheric transport and stratosphere-troposphere exchange, *J. Geophys. Res.*, *108*(D8), 4234, doi:10.1029/2002JD002395.

Kritz, M. A., S. W. Rosner, E. F. Danielsen, and H. B. Selkirk (1991), Air mass origins and troposphere-to-stratosphere exchange associated with mid-latitude cyclogenesis and tropopause folding inferred from ^{7}Be measurements, *J. Geophys. Res.*, *96*(D9), 17,405–17,414, doi:10.1029/91JD01358.

Lal, D., and B. Peters (1967), Cosmic ray produced radioactivity on the earth, in *Handbuch der Physik,* vol. 46/2, edited by K. Sittle, pp. 551–612, Springler, Berlin.

Lal, D., P. K. Malhotra, and B. Peters (1958), On the production of radioisotopes in the atmosphere by cosmic radiation and their application to meteorology, *J. Atmos. Terr. Phys*, *12*(4), 306–328.

Lefohn, A. S., H. Wernli, D. Shadwick, S. Limbach, S. J. Oltmans, and M. Shapiro (2011), The importance of stratospheric–tropospheric transport in affecting surface ozone concentrations in the western and northern tier of the United States, *Atmos. Environ.*, *45*(28), 4845–4857.

Logan, J. A. (1985), Tropospheric ozone: Seasonal behavior, trends, and anthropogenic influence, *J. Geophys. Res.*, *90*(D6), 10,463–10,482, doi:10.1029/JD090iD06p10463.

Paillard, D., L. Labeyrie, and P. Yiou (1996), Macintosh program performs time-series analysis, *Eos Trans. AGU*, *77*(39), 379–379.

Peake, E., and B. D. Fong (1990), Ozone concentrations at a remote mountain site and at two regional locations in southwestern Alberta, *Atmos. Environ. A-Gen.*, *24*(3), 475–480, doi:10.1016/0960-1686(90)90004-7.

Pudykiewicz, J. (1989), Simulation of the Chernobyl dispersion with a 3-D hemispheric tracer model, *Tellus Ser. B*, *41B*(4), 391–412, doi:10.1111/j.1600-0889.1989.tb00317.x.

Pudykiewicz, J. (1998), Application of adjoint tracer transport equations for evaluating source parameters, *Atmos. Environ.*, *32*(17), 3039–3050, doi:10.1016/S1352-2310(97)00480-9.

Seibert, P., and A. Frank (2004), Source-receptor matrix calculation with a Lagrangian particle dispersion model in backward mode, *Atmos. Chem. Phys.*, *4*(1), 51–63, doi:10.1016/0960-1686(90)90004-7.

Sparks, R., M. Bursik, S. Carey, J. Gilbert, L. Glaze, H. Sigurdsson, and A. Woods (1997), *Volcanic Plumes*, John Wiley & Sons, Baffin Lane, Chichester, West Sussex PO19 1UD, England.

Stohl, A., H. Wernli, P. James, M. Bourqui, C. Forster, M. A. Liniger, P. Seibert, and M. Sprenger (2003), A new perspective of stratosphere–troposphere exchange, *Bull. Am. Meteorol. Soc.*, *84*(11), 1565–1573, doi:10.1175/BAMS-84-11-1565.

Stohl, A., et al. (2000), The influence of stratospheric intrusions on alpine ozone concentrations, *Atmos. Environ.*, *34*(9), 1323–1354, doi:10.1016/S1352-2310(99)00320-9.

Usoskin, I. G., and G. A. Kovaltsov (2008), Production of cosmogenic ^{7}Be isotope in the atmosphere: Full 3-D modeling, *J. Geophys. Res.*, *113*, D12107, doi:10.1029/2007JD009725.

Usoskin, I. G., C. V. Field, G. A. Schmidt, A.-P. Leppänen, A. Aldahan, G. A. Kovaltsov, G. Possnert, and R. K. Ungar (2009), Short-term production and synoptic influences on atmospheric ^{7}Be concentrations, *J. Geophys. Res.*, *114*, D06108, doi:10.1029/2008JD011333.

van Dop, H., F. T. M. Nieuwstadt, and J. C. R. Hunt (1985), Random walk models for particle displacements in inhomogeneous unsteady turbulent flows, *Physics of Fluids (00319171)*, *28*(6), 1639–1653.

Vautard, R., and M. Ghil (1989), Singular spectrum analysis in nonlinear dynamics, with applications to paleoclimatic time series, *Physica D*, *35*(3), 395–424, doi:10.1016/0167-2789(89)90077-8.

Wilson, J., F. Ferrandino, and G. Thurtell (1989), A relationship between deposition velocity and trajectory reflection probability for use in stochastic Lagrangian dispersion models, *Agric. For. Meteorol.*, *47*(2-4), 139–154, doi:10.1016/0168-1923(89)90092-0.

Wilson, J. D., and B. L. Sawford (1996), Review of Lagrangian stochastic models for trajectories in the turbulent atmosphere, *Boundary Layer Meteorol.*, *78*(1), 191–210, doi:10.1007/BF00122492.

Wotawa, G., et al. (2003), Atmospheric transport modelling in support of CTBT verification—Overview and basic concepts, *Atmos. Environ.*, *37*(18), 2529–2537, doi:10.1016/S1352-2310(03)00154-7.

Zanis, P., et al. (2003a), An estimate of the impact of stratosphere-to-troposphere transport (STT) on the lower free tropospheric ozone over the Alps using ^{10}Be and ^{7}Be measurements, *J. Geophys. Res.*, *108*(D12), 8520, doi:10.1029/2002JD002604.

Zanis, P., et al. (2003b), Forecast, observation and modelling of a deep stratospheric intrusion event over Europe, *Atmos. Chem. Phys. Discuss.*, *3*(1), 1109–1138.

Zheng, X., C. Shen, G. Wan, K. Liu, J. Tang, and X. Xu (2011), ^{10}Be/^{7}Be implies the contribution of stratosphere-troposphere transport to the winter-spring surface O_3 variation observed on the Tibetan Plateau, *Chin. Sci. Bull.*, *56*(1), 84–88.